

Full length article

Plasma-enhanced atomic layer deposition of barium titanate with aluminum incorporation



Yongmin Kim^a, Peter Schindler^a, Anup L. Dadlani^b, Shinjita Acharya^a, J. Provine^a, Jihwan An^{a, c, *}, Fritz B. Prinz^{a, d}

^a Department of Mechanical Engineering, Stanford University, Stanford, CA 94305, USA

^b Department of Chemistry, Stanford University, Stanford, CA 94305, USA

^c Manufacturing Systems and Design Engineering Programme, Seoul National University of Science and Technology, Seoul 139-743, South Korea

^d Department of Materials Science and Engineering, Stanford University, Stanford, CA 94305, USA

ARTICLE INFO

Article history:

Received 3 February 2016

Received in revised form

4 July 2016

Accepted 6 July 2016

Keywords:

High-k thin films

Doped barium titanate

Plasma-enhanced ALD

DRAM capacitor

ABSTRACT

Plasma-enhanced atomic layer deposition (PEALD) of ultrathin (~7 nm) slightly Ti-rich $\text{Ba}_x\text{Ti}_y\text{O}_z$ (BTO) films with different Al-doping concentration ($[\text{Al}]/([\text{Al}] + [\text{Ba}] + [\text{Ti}]) = 0$ to 22 at%) was studied. In particular, the effects of Al-doping in BTO on compositional, crystallographic and electrical properties were investigated. Previously, BTO films with a Ti cation composition, $[\text{Ti}]/([\text{Ba}] + [\text{Ti}]) = \sim 60$ at% was reported to be advantageous for crystallization, resulting in superior dielectric properties. These Ti-rich BTO films, however, suffered from high leakage currents, necessitating the change in its crystalline structure as well as elemental composition. By incorporating Al_2O_3 into the BTO films, the leakage current can be controlled, where the BTO films with an Al-doping concentration of 12 at% showed a leakage current reduced by one order of magnitude compared to un-doped BTO (i.e., $\sim 10^{-7}$ to $\sim 10^{-6}$ A/cm² at +1.6 V) without a significant drop of the dielectric constant (43, un-doped to 40, Al-doped).

© 2016 Acta Materialia Inc. Published by Elsevier Ltd. All rights reserved.

1. Introduction

Dielectric films with high dielectric constants (i.e., high-k) and low leakage currents are essential for the applications of information storage devices (e.g. dynamic random access memory (DRAM)) [1]. As the feature size shrinks to enable a higher degree of storage capacity, DRAM industries demand next-generation high-k materials over conventional dielectric materials based on ZrO_2 , HfO_2 , and Ta_2O_5 which have already approached their intrinsic limits in material properties. In that regard, M-doped TiO_2 ($M = \text{Al}, \text{Hf}$) [2–4] and perovskite-type $\text{A}_x\text{Ti}_y\text{O}_z$ ($A = \text{Sr}, \text{Ba}, (\text{Ba}, \text{Sr})$) have been newly highlighted because i) crystallized TiO_2 intrinsically possesses high dielectric constants (ϵ) (anatase, 30–40; rutile, 83–100) [5], ii) incorporation of other cations such as Sr, Ba, and La further increases ϵ values by formation of perovskite structures, and iii) the reduction in leakage current is highly feasible by incorporation of these high band gap materials (BaO, 4.8 eV; La_2O_3 , 5.8 eV; SrO,

6.5 eV; Al_2O_3 , 8.8 eV) [4,6,7].

Atomic layer deposition (ALD) offers unique features for developing high quality ultra-thin dielectric films compared to other deposition techniques. The self-limiting nature of ALD enables the deposition of pin-hole free and conformal layers, even suitable for deep-trench structures which have been widely used in the microelectronics industry [8]. In particular, O_2 plasma-enhanced ALD (PEALD) has proved its capability to deposit ultrathin BaTiO_3 films as well as modulating its crystallinity [9,10]: O_2 PEALD is an energy-enhanced variant of ALD which utilizes oxygen plasma species as an oxidizer instead of water vapor widely used for conventional thermal ALD (T-ALD) [11]. Plasma generators using microwave plasma, electron cyclotron resonance plasma, or RF-driven inductively-coupled plasma (ICP) create O_2 radical species which renders greater flexibility in processing conditions and a wider range of materials to use in comparison to the conventional T-ALD [11]. Previously, we reported the deposition of ultra-thin $\text{Ba}_x\text{Ti}_y\text{O}_z$ (BTO) films with different Ba/Ti ratios using a commercialized PEALD station equipped with the RF-ICP generator, the FlexAL system (Oxford Instruments) [10]. Interestingly, BTO films with higher Ti content than Ba showed larger dielectric constants compared to other Ba-to-Ti stoichiometries (while other deposition conditions

* Corresponding author. Manufacturing Systems and Design Engineering (MSDE) Programme, Seoul National University of Science and Technology, Seoul 139-743, South Korea

E-mail address: jihwanan@seoultech.ac.kr (J. An).

were kept the same) [10]. One plausible explanation for the higher dielectric constants is that Ti-rich BTO films are more likely to induce crystallized grains inside of the thin films (under the same plasma power and duration), eventually beneficial for improving throughput. The Ti-rich BTO film, however, suffers from higher leakage currents due to the existence of grain boundaries formed during the crystallization process [4].

One of the promising approaches to minimize leakage currents as well as sustaining the intrinsic benefits of Ti-rich BTO films, described above, is the doping of higher band gap (E_g) material into the thin films. Previously, Sn_2O_3 doping into BTO (>0.4 wt%) showed an anomalous increase in electrical resistivity, resulting in a highly insulating dielectric [12]. Another oxide, Al_2O_3 with the same oxidation number of +3 as Sn_2O_3 , proved its effectiveness to reduce leakage currents when it was doped into TiO_2 [4], ZrO_2 [13–16], and HfO_2 [13]. Especially, the concept of Al_2O_3 incorporation into ZrO_2 , widely known as the $\text{ZrO}_2/\text{Al}_2\text{O}_3/\text{ZrO}_2$ (ZAZ)-type dielectric has been realized in DRAMs down to 45 nm pitch size due to the following benefits: ZAZ achieves a moderate dielectric constant ($\epsilon = \sim 39$) while obtaining a low leakage current ($2.11 \times 10^{-6} \text{ A/cm}^2$ at +2 V) by controlling crystallization to a moderate amount, i.e., intermixing of crystalline and amorphous phases, which suppresses the formation of pathways for electrical leakage. However, even for increasingly integrated DRAM architectures where enlarged electrodes based on the concept of trench-type capacitors will no longer be used, alternative materials with higher dielectric constants ($\epsilon > 40$) should be utilized [17].

In this study, we demonstrate the PEALD of Al-doped BTO thin films with high dielectric constants (up to ~ 43) and the ability to tune the dielectric constant as well as electric leakage currents by i) modulating the amount of Al-doping and ii) facilitating oxygen plasma as a post-treatment. Based on the observations of the changes in crystallinity and electronic structures, we conclude that Al-doping plays a crucial role in controlling the crystallinity, where a trade-off between dielectric constants and leakage currents exists, similar to the ZAZ dielectric case. Despite this trade-off, Al-doping into BTO showed considerable reduction in leakage currents with a minimal sacrifice of the dielectric constants.

2. Experimental

The detailed description of BTO and Al_2O_3 PEALD conditions in a commercial PEALD station (Oxford, FlexAL) was reported elsewhere [10,18]. The atomic percentage of Al in the BTO films was controlled by varying the Al_2O_3 and BTO deposition cycle ratio ([number of Al-O cycles]/[number of Al-O cycles + number of BTO cycles]). Ba-to-Ti pulse ratio was 1:5 in one super-cycle, and the BTO deposition with 15 super-cycles was conducted. Under this deposition condition, Ti-rich BTO films ([Ti]/([Ba]+[Ti]) = 60–67 at%) were deposited. For Al-doped BTO films, additional Al_2O_3 deposition cycle composed of TMA pulsing/purging followed by O_2 plasma pulsing/purging were carried out with the BTO PEALD process. x TMA BTO ($x = 0, 3, 5$, and 8) means that Al-O layers with the number of x were inserted with an even distribution within the BTO films with 15 super-cycle deposition. Due to the added Al-O deposition sequence, the thickness values of the BTO films with different Al content were measured in the range of 6.5–7.2 nm measured by the transmission electron microscope (TEM) (see below).

To enhance the crystallinity of Al-doped BTO films and repair lattice damage/defects, O_2 plasma-treatment for 3 h (plasma power, 400 W; plasma pressure, 5 mTorr) was performed after the deposition of the BTO films in an O_2 atmosphere (Praxair, purity grade 4.8). The post O_2 plasma treatment is advantageous over rapid thermal annealing (RTA) due to its lower process temperature, which is below 400 °C: An et al. previously observed a

significant enhancement in crystallinity from T-ALD BTO grown at 250 °C via post plasma treatment by using a remote oxygen plasma (type, ICP; plasma power, 250 W; plasma pressure, 15 mTorr) [9]. As a result, all post-treated samples, un-doped and Al-doped BTO films showed nearly stoichiometric O concentration, ~ 60 at% throughout the BTO films (Fig. S1), in contrast to as-deposited films with an O concentration of ~ 55 at%. This is due to the oxygen replenishment of the oxygen vacancy sites, resulting in the reduction of the Poole-Frenkel (P-F) emission dominated leakage current (see below) [19–21]. All oxygen-plasma-treated samples showed low carbon contamination in the film under the X-ray Photoemission Spectroscopy (XPS) detectable limit (<1 at%) after removing surface carbon on every sample (generated during transfer process) by using 0.1 min Ar^+ -ion etching (voltage, 2 kV; current, 1 μA ; size, 2 $\mu\text{m} \times 2 \mu\text{m}$; calibrated sputtering rate on SiO_2 , 5 nm/min). Although the employed long post plasma treatment (3 h) seems to be impractical as viewed from increasing throughput, the reduction of the post process time could be possible by utilizing a higher energy plasma source.

As the first step to fabricate the metal-insulator-metal (MIM) structures, bottom electrodes, 20 nm Zr-doped TiN (Zr-TiN) was deposited on thermally-grown SiO_2 (200 Å)/p-Si using a PEALD station (Fiji, Cambridge Nanotech/Ultratech): The more detailed fabrication process is described in the supporting information. The Zr doping into TiN is beneficial in terms of a higher resistance against oxygen diffusion [22]: Zr atoms can effectively reduce oxygen diffusion toward TiN, leading to a reduced formation of an interfacial oxide layer that does not negatively affect the work function. It should be noted that the work function of Zr-doped TiN ($\Phi_{\text{Zr-TiN}}$), measured to be 5.0 eV, was higher than the work function of un-doped TiN (Φ_{TiN}), 4.7 eV [23,24]. After fabrication of the Al-doped BTO/ZrTiN stacking structure, rectangular-shaped Pt top electrodes (area, 0.75 mm \times 0.75 mm; thickness, 200 nm) were patterned by DC sputtering for electrical measurement. The thickness and crystallinity of the films were investigated by high-resolution TEM (HRTEM, FEI Titan 80–300 Environmental TEM). Atomic force microscope (AFM, JEOL 5200) was used to characterize the surface topography as well as root-mean-square (RMS) roughness values of each case: 2–3 different spots with the window size of 1 $\mu\text{m} \times 1 \mu\text{m}$ were taken into account for quantification of average roughness. The composition analyses and the chemical binding states were conducted by X-ray Photoelectron Spectroscopy (XPS, PHI VersaProbe Scanning XPS Microscope) with Al ($K\alpha$) radiation (1486 eV), followed by surface cleaning by Ar^+ -ion etching, showing a negligible carbon impurity below the detection limit (<1 at%). Angle-resolved XPS (ARXPS) measurements were carried out to obtain high resolution compositional depth profiles and the samples were rotated to 75° from its original surface plane to achieve a grazing angle. The valence band offsets ($E_{\text{vac}} - E_v$) of un-doped and Al-doped BTO on Zr-doped TiN, determined by the difference between the vacuum-level energy and the valence band maximum as well as the work functions of the electrodes (e.g. Pt and Zr-doped TiN) were measured by ultraviolet photoemission spectroscopy (UPS) in air (UPS with a model AC-2 Photoelectron Spectrometer at atmospheric pressure, using a deuterium UV source in air). Optical band gap measurements were performed by an UV-vis spectrometer (PerkinElmer Lambda 1050) using extrapolation to x -intercepts in Tauc plots for as-deposited and plasma-treated samples with different Al contents (Fig. S2) to obtain the band gap. The capacitance-frequency (C-f) was measured using a LCR meter (Agilent, model no. E4980A) at 0 V DC bias voltage and the dielectric constants were measured at a frequency of 1 kHz. The applied voltage-current density (V-J) characteristics were measured from 0 to +1.8 V bias, using a Keithley 2636A Source-meter. To measure the bulk dielectric constant (ϵ) while ruling

out the effect of the interfacial layer, other sets of samples with a higher number of super-cycles (number of super-cycles, corresponding thickness ranges; 22, 9.5–10.6 nm; 30, 13–14.4 nm), was fabricated and the slopes of the curve of dielectric constant allowed for extraction of physical thickness, similar to the previous report [4].

3. Results and discussion

Fig. 1a shows ARXPS depth profile analyses for the un-doped BTO (15 super-cycles of BTO, Ba-to-Ti pulse ratio = 1:5). Atomic signals from BTO appeared with less contribution from the underlying Zr-TiN electrodes during sputtering with Ar^+ ions from 0 to 0.6 min and Ti-rich cation composition at $[\text{Ti}]/([\text{Ba}] + [\text{Ti}]) = 61\text{--}67\text{ at\%}$ was confirmed. Note that erratically high C atomic signal at 0 min was affected by surface carbon while higher Ti concentration ($[\text{Ti}]/([\text{Ba}] + [\text{Ti}]) > 70\text{ at\%}$) was observed at > 0.75 min sputtering time, resulted from the underlying ZrTiN substrate. For the Al-doped BTO films, by simply adding Al-O deposition sequence into the BTO deposition, the overall $[\text{Al}]/([\text{Al}] + [\text{Ba}] + [\text{Ti}])$ atomic ratios of the Al-doped BTO films with x TMA cycles ($x = 0, 3, 5, \text{ and } 8$) were 0, 8, 12, and 22 at%, respectively. Hence, Al content was linearly controlled with the number of TMA cycles (Fig. 1b) with R-squared value of 0.9918. All Al-doped BTO samples showed a similar Ti-rich composition, confirmed by ARXPS depth profiles (Fig. S1).

The effects of Al-doping on crystallization are presented by several cross-sectional HRTEM images in Fig. 2. The amount of Al-doping indicates clear relevance with the change in the degree of crystallization, as similar to $\text{ZrO}_2/\text{Al}_2\text{O}_3/\text{ZrO}_2$ laminate structure [14,15]. Fig. 2a and b showed the as-deposited and plasma treated BTO without doping, respectively: Oxygen plasma significantly increased the crystallized area which leads to a significantly enhanced dielectric constant (*see below*). It should be noted that areas circled with white dotted lines clearly showed lattice fringes: Lattice spacings in the crystalline area are measured at 1.46 Å corresponding well with (220) type planes in either cubic or tetragonal BTO (inter-planar angle, 60°). The root-mean-square (RMS) roughness decreased from 0.37 nm (as-deposited, un-doped) to 0.24 nm (plasma treatment, un-doped), which is also indicative of crystallization accompanied by film densification (Fig. S3). An et al. suggested that the lower roughness of plasma-treated samples centers in the motion of surface adatoms into

surface pores excited by ions, hence smoothing the surface [9]. Fig. 2c, d, and e showed HRTEMs of plasma-treated Al-doped BTO with 3, 5, and 8 TMA cycles and the total crystallized area encircled by the white dotted line tends to decrease with more addition of aluminum into the film. The phenomenon that increased Al-doping impedes the crystallization process more, has been similarly observed in previous reports of Al-doping into ZrO_2 , HfO_2 , and TiO_2 [4,13].

In the cases of Al-doped BTO, AFM studies showed the RMS roughness values of Al-doping (3 TMA and 5 TMA) were slightly increased while Al-doped BTO with 8 TMA became significantly roughened after plasma treatment (Fig. S3e). Note that the increase in the RMS roughness of the plasma-treated samples with more Al-doping (black rectangle) could not be only related to the behavior of crystallization for Al-doped samples: It could arise out of the segregation of Al from the BTO film, more severe in the higher Al-content sample (i.e. 8 TMA), which was also reported elsewhere [4]. The increase of metallic Al (Al2p, 73 eV) on the surface of Al-doped BTO with 8 TMA confirmed by ARXPS again confirmed segregation behavior of Al onto the surface (Fig. S4).

The variations in the dielectric constants (ϵ) of the un-doped and Al-doped BTO films with various Al doping ratios are shown in the Fig. 3a. The ϵ values of as-deposited BTO films were ~ 11 regardless of Al content, which lies in between the previously reported permittivity value (15) of amorphous BTO and the permittivity value (7.7) of amorphous Al_2O_3 [25,26]. After being post-treated with O_2 plasma, the ϵ values were significantly enhanced (black rectangles in Fig. 2a). The improvement in the ϵ values could be explained by the formation of 1–3 nm sized crystalline BTO grains, confirmed by the encircled areas in the HRTEM micrographs in Fig. 2. A trend between ϵ and Al content was clearly observed: The effect of Al incorporation with $[\text{Al}]/([\text{Al}] + [\text{Ba}] + [\text{Ti}]) < 8\%$ showed negligible effect on the change of ϵ , however, BTO films with higher Al contents $[\text{Al}]/([\text{Al}] + [\text{Ba}] + [\text{Ti}]) > 8\%$ showed lower permittivity values (10% drop in ϵ for $[\text{Al}]/([\text{Al}] + [\text{Ba}] + [\text{Ti}]) = 12\text{ at\%}$ and 44% drop in ϵ for $[\text{Al}]/([\text{Al}] + [\text{Ba}] + [\text{Ti}]) = 22\text{ at\%}$). This observation is consistent with the evolution of ϵ values for Al-doped TiO_2 (ATO) depending on Al content, i.e., higher Al doping ($> 10\text{ at\%}$ with respect to the total amount of cations) results in lower ϵ values due to lower polarization of Ti-O-Al and formation of ~ 1 nm thick interfacial Al_2O_3 oxide layer segregated from ATO [4]. ZrO_2 and Al_2O_3 mixed structure, ZAZ dielectric also showed a similar trend of ϵ governed by Al content: The ZrO_2 crystallization is significantly

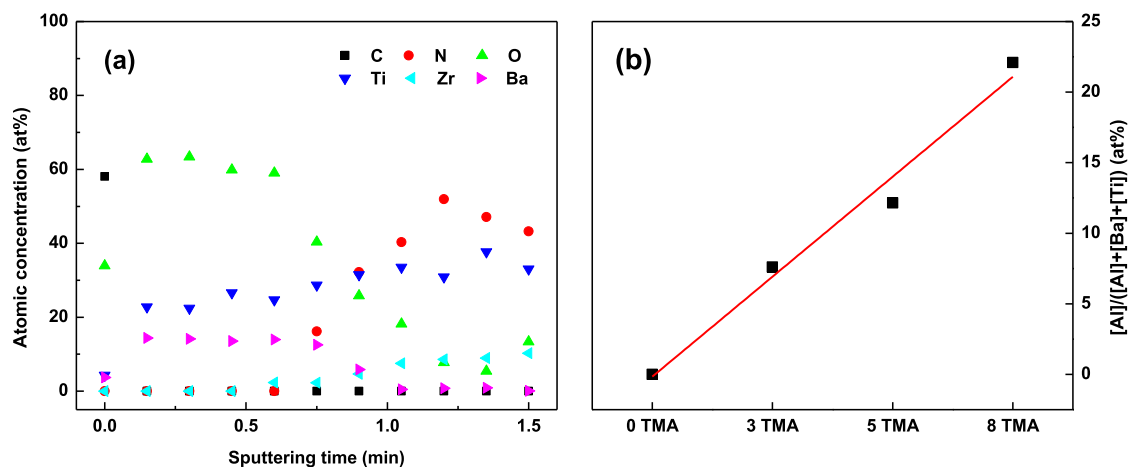


Fig. 1. (a) ARXPS depth profile of un-doped BTO film after 3 h of oxygen plasma treatment and (b) XPS-measured $[\text{Al}]/([\text{Al}] + [\text{Ba}] + [\text{Ti}])$ atomic ratios of several Al-doped BTO films, integrated from the surface to the depth of > 5 nm, while the red line indicating a linear regression line. (For interpretation of the references to colour in this figure legend, the reader is referred to the web version of this article.)

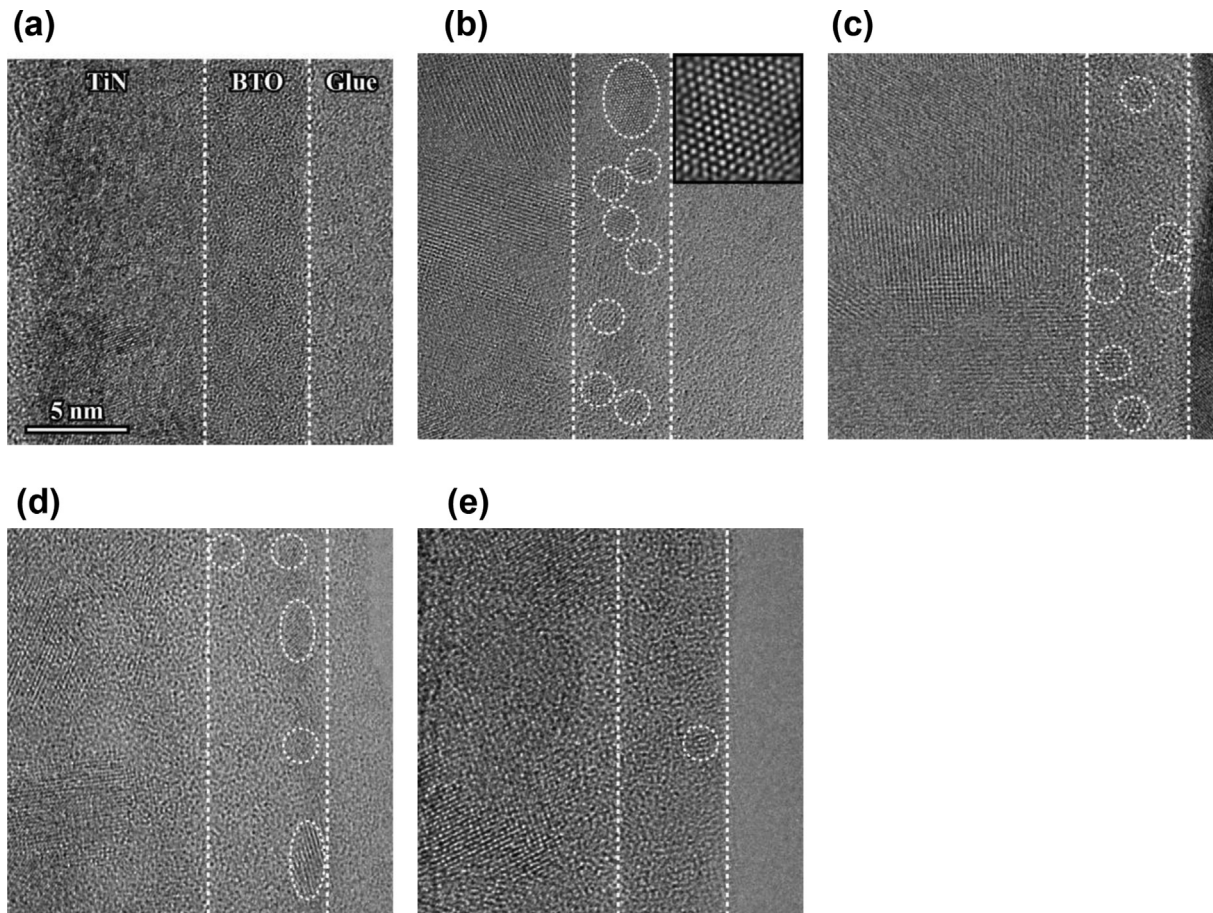


Fig. 2. HRTEM of un-doped and Al-doped BTO (x cycles of TMA in 15 super-cycles of BTO, $x = 0, 3, 5,$ and 8): as-deposited (a) and after O_2 plasma post treatment (b, c, d, and e). (a, b) 0 TMA (inset, zoomed images of the region showing lattice fringes encircled by the white dotted lines), (c) 3 TMA, (d) 5 TMA, and (e) 8 TMA. The crystallinity in white-dotted-line encircled area was confirmed in TEM FFT mode. The scale bar in Fig. 2a is also applicable for other TEM images.

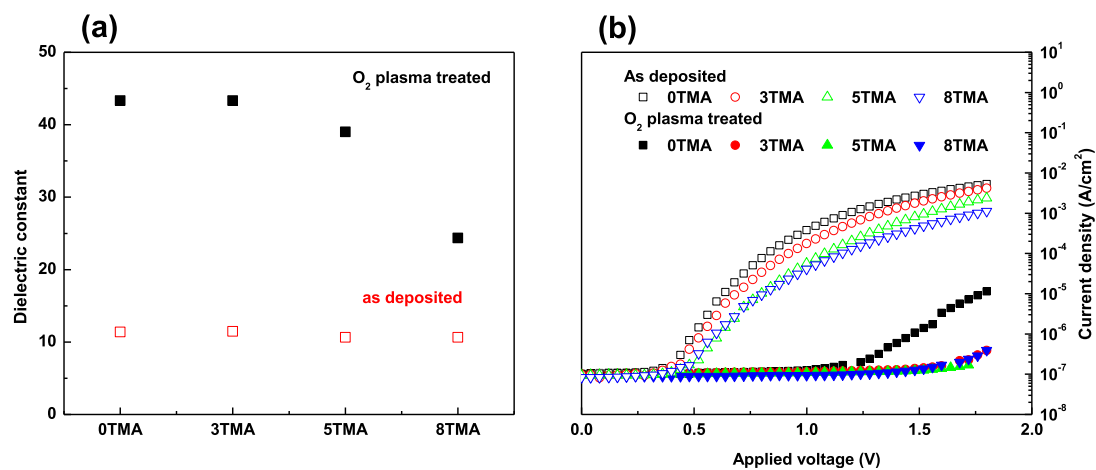


Fig. 3. Electrical properties of un-doped and Al-doped BTO (x cycles of TMA in 15 super-cycles of BTO, $x = 0, 3, 5,$ and 8): (a) the dielectric constants and (b) the leakage current density (J-V) curves. (Open squares represent as-deposited samples and closed square represent O_2 -plasma treated samples.)

deterred by the insertion of Al_2O_3 , leading to a drop in ϵ [14,15]. Capacitance-voltage (C-V) characteristics at 1 kHz of the un-doped and Al-doped BTO films (0 and 5 TMA) after O_2 plasma treatment shown in Fig. S6 proves no hysteresis on the films with some crystallinity. C-V hysteresis, a characteristic of crystalline ferroelectric films, does not happen in the films with crystallites

embedded in amorphous matrix, presumably due to the dominance of amorphous nature of the film [27,28].

The leakage-current (J-V) density behavior of un-doped and Al-doped BTO films are shown in Fig. 3b. Leakage current densities under positive bias at the top Pt represent the quantity of electrons injected from the bottom Zr-TiN (Φ_{Zr-TiN} , 5.0 eV) to the dielectric

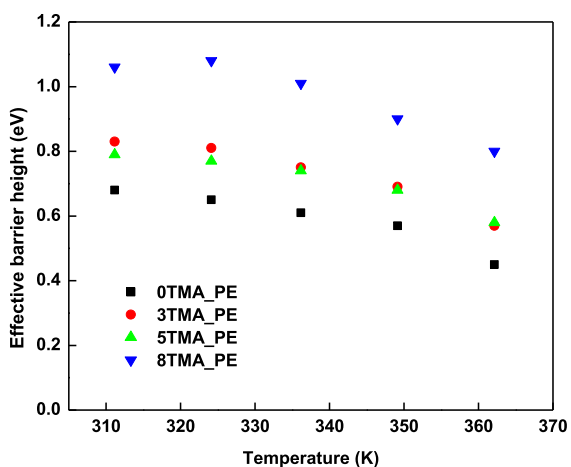


Fig. 4. Effective barrier heights (eV) at the interface of (un-doped or Al-doped) BTO and Zr-doped TiN depending on aluminum doping quantity, x TMA ($x = 0, 3, 5,$ and 8) at different temperatures (311–362 K). All BTO layers were oxygen-plasma-treated.

layers. All as-deposited BTO films showed high J values at $+1.6$ V (10^{-4} – 10^{-2} Acm $^{-2}$) which could be explained by the oxygen-vacancy-assisted P-F tunneling (recalling that as-deposited BTO contained 8% less oxygen than plasma-treated). O $_2$ -plasma-treated samples, however, showed a significant delay in onset of the J -value rise from the base line at $\sim 10^{-7}$ A/cm 2 , i.e., onset shifted from 0.5 V (as-deposited) to > 1 V and showed the linear behavior at this high voltage range, which has been well explained by the F-N tunneling behavior, rather than the Schottky or the P-F emission mechanism (detailed explanation included in the supporting information, Figs. S5–S8). The resulting barrier height values of the plasma treated samples, Φ_B , was obtained from the fitting of J - V curves at high voltage to the F-N tunneling model, are shown in Fig. 4, and they display a strong dependence on Al-doping as well as temperature. At 311 K, Al-doping increases Φ_B from 0.68 eV (un-doped BTO) to 0.79–0.83 eV (3 TMA and 5 TMA); Al-doped BTO with 8 TMA showed Φ_B of 1.06 eV, significantly higher than the lower-doping cases, presumably originating from the segregation of Al at the interface followed by the formation of an additional barrier layer (*see above*). The dependence of Φ_B on temperature is indicative of the contribution of the trap-assisted-tunneling (TAT) mechanism: The decrease in Φ_B has been understood as an increase

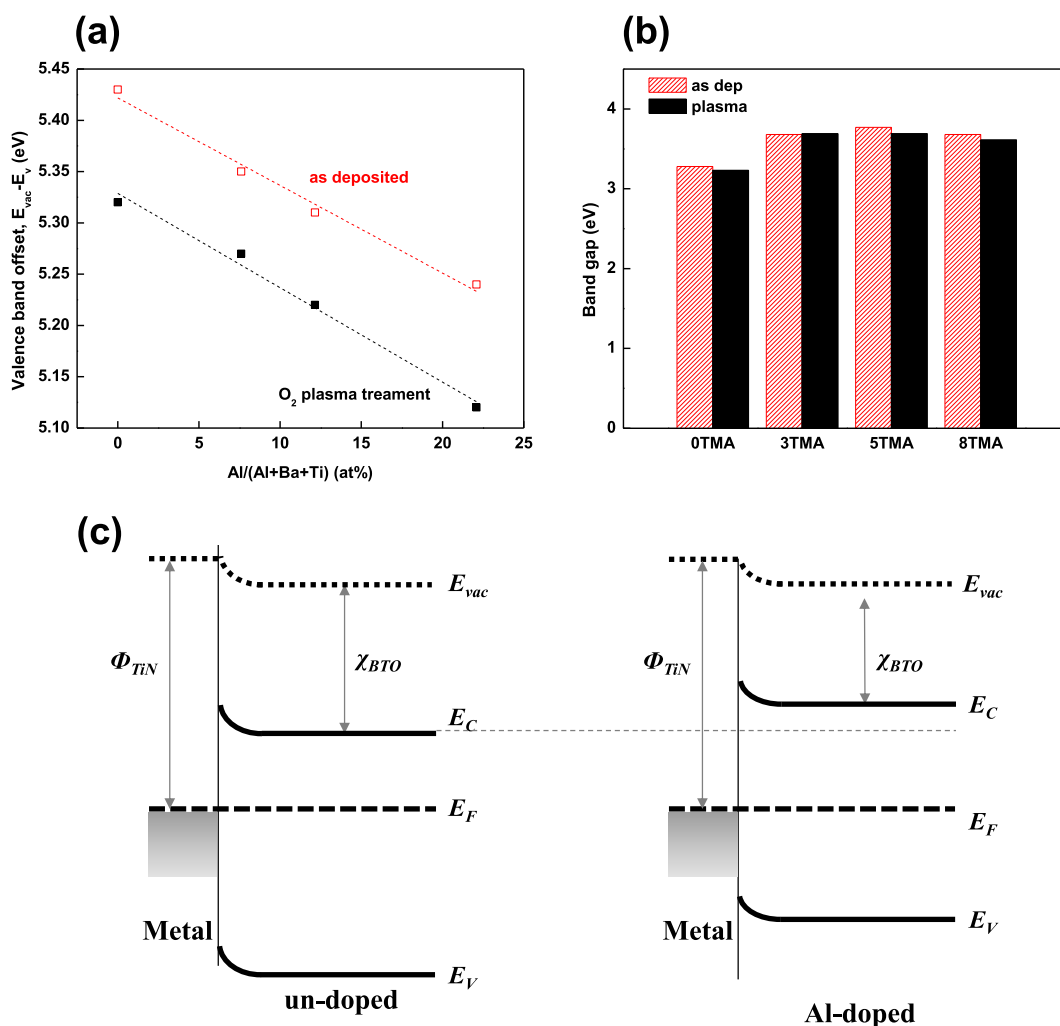


Fig. 5. (a) Variation of valence band offset (VBO, $E_{vac} - E_v$) values measured by UPS (black closed, oxygen-plasma-treated; red open, as-deposited), (b) band gap variation measured by UV-vis (black closed, oxygen-plasma-treated; red diagonal patterned, as-deposited) and (c) the schematic representation of the band structures of un-doped BTO and Al-doped BTO. (For interpretation of the references to colour in this figure legend, the reader is referred to the web version of this article.)

in the trap density at a lower energy level resulting from a thermal excitation of electrons [13].

Other spectrometric evidences – the valence band offset (VBO, $E_{\text{vac}}-E_{\text{v}}$) and band gap (E_{g}) measured by UPS and UV-vis, respectively – support the Al-doped-assisted modulation of Φ_{B} (Fig. 5). It was confirmed that Al-doping increases the conduction band offset (CBO, $E_{\text{vac}}-E_{\text{c}}$), equal to ($E_{\text{vac}}-E_{\text{v}}$) minus by E_{gs} , which in turn (for the case of an unchanged or increased E_{g}) results in a higher Φ_{B} . The VBOs for the as-deposited BTO samples with x TMA cycles ($x = 0, 3, 5$, and 8) are 5.43, 5.35, 5.31, and 5.24 (eV), respectively. O_2 -plasma-treated samples shifted the VBOs to lower values presumably due to annihilation of trap states by incorporating oxygen atoms. Al-doping further decreased the VBOs: The VBOs of the BTO with x TMA cycles ($x = 0, 3, 5, 8$) are 5.32, 5.27, 5.22, and 5.12 (eV), respectively, as shown in Fig. 4a. In addition, the decrease in the VBOs is not the only factor, but the increase in E_{g} by Al-doping also contributes to the increase in barrier height (Fig. 5b). Initially with increasing Al content, the covalency of the system increases, which means the band gap of Al-doped BTO tends to increase towards that of alumina, 6.6–7 eV [6,27]. However, as increasing the Al content significantly, the Ti–O bonds are likely being stretched. This elongation of Ti–O indicates the increase in the ionicity of Ti, generally accompanied by a decrease in band gap. Hence we see the band gap first increase with the initial introduction of Al, but when the concentration reaches some threshold, the trend is reversed and band gap again decreases. Overall E_{g} values were increased by Al-doping: E_{g} values for O_2 -plasma-treated samples are increased from 3.23 eV (0 TMA) to 3.69, 3.76, and 3.61 eV for 3, 5 and 8 TMA, respectively. The combination of increased E_{g} and decreased VBO finally results in the reduced CBO of the BTO film, alternatively, a decrease in electron affinity of BTO (X_{BTO} , 2.09, 1.66, 1.46, and 1.51 eV for 0, 3, 5, and 8 TMA). This results in an increased barrier height between the bottom electron and the BTO layer, $\Phi_{\text{B}} = (\Phi_{\text{TIN}}-X_{\text{BTO}})$.

4. Conclusion

Al-doped BTO films were successfully fabricated by the PEALD and demonstrated its potential as dielectric materials with promising electrical properties with a dielectric constant ~ 43 and leakage current of $\sim 10^{-7}$ A/cm² at +1.6 V. It was also confirmed that plasma-treated Al-doped BTO on a different substrate such as a RuO_2 , which is highly conductive quasimetallic with less chance to form interfacial dielectric layer [28], shows similar dielectric constant of ~ 42 at 1 kHz (Fig. S9). The aforementioned achievements were enabled by the fine tuning of crystallinity and chemical composition of the ultrathin films (~ 7 nm), which could only be realized by PEALD. Our results, which simultaneously modulate the dielectric constant and the leakage current density of thin films, may have significant implications not only on next-generation DRAMs but also on a wider range of emerging technologies such as energy storage devices and displays.

Acknowledgments

The authors sincerely appreciate the Manufacturing Technology Center, Samsung Electronics Co., Ltd., for financial support. Part of this work was performed using the FEI Titan 300 kV ETEM and the PHI VersaProbe Scanning XPS Microscope at the Stanford Nano Shared Facilities (SNSF). J. An also acknowledges financial support from the National Research Foundation of the Korean Ministry of Education, Science and Technology (Grant No. NRF-2015R1D1A1A01058963).

Appendix A. Supplementary data

Supplementary data related to this article can be found at <http://dx.doi.org/10.1016/j.actamat.2016.07.018>.

References

- [1] A.I. Kingon, J.-P. Maria, S.K. Streiffer, Alternative dielectrics to silicon dioxide for memory and logic devices, *Nature* 406 (2000) 1032–1038, <http://dx.doi.org/10.1038/35023243>.
- [2] M. Seo, S.K. Kim, J.H. Han, C.S. Hwang, Permittivity enhanced atomic layer deposited HfO₂ thin films manipulated by a rutile TiO₂ interlayer, *Chem. Mater.* 22 (2010) 4419–4425, <http://dx.doi.org/10.1021/cm1010289>.
- [3] M. Seo, S.H. Rha, S.K. Kim, J.H. Han, W. Lee, S. Han, et al., The mechanism for the suppression of leakage current in high dielectric TiO₂ thin films by adopting ultra-thin HfO₂ films for memory application, *J. Appl. Phys.* 110 (2011) 024105, <http://dx.doi.org/10.1063/1.3605527>.
- [4] S.K. Kim, G.-J. Choi, S.Y. Lee, M. Seo, S.W. Lee, J.H. Han, et al., Al-Doped TiO₂ films with ultralow leakage currents for next generation DRAM capacitors, *Adv. Mater.* 20 (2008) 1429–1435, <http://dx.doi.org/10.1002/adma.200701085>.
- [5] S.K. Kim, W.-D. Kim, K.-M. Kim, C.S. Hwang, J. Jeong, High dielectric constant TiO₂ thin films on a Ru electrode grown at 250 °C by atomic-layer deposition, *Appl. Phys. Lett.* 85 (2004) 4112–4114, <http://dx.doi.org/10.1063/1.1812832>.
- [6] R.R. Reddy, Y. Nazeer Ahammed, K. Rama Gopal, D.V. Raghuram, Optical electronegativity and refractive index of materials, *Opt. Mater.* 10 (1998) 95–100, [http://dx.doi.org/10.1016/S0925-3467\(97\)00171-7](http://dx.doi.org/10.1016/S0925-3467(97)00171-7).
- [7] G. Scarel, A. Svane, M. Fanciulli, Scientific and technological issues related to rare earth oxides: an introduction, in: M. Fanciulli, G. Scarel (Eds.), *Rare Earth Oxide Thin Films*, Springer, Berlin Heidelberg, 2007, pp. 1–14 (accessed 1.02.15), http://link.springer.com/chapter/10.1007/11499893_1.
- [8] P. Schindler, M. Logar, J. Provine, F.B. Prinz, Enhanced step coverage of TiO₂ deposited on high aspect ratio surfaces by plasma-enhanced atomic layer deposition, *Langmuir* 31 (2015) 5057–5062, <http://dx.doi.org/10.1021/acs.langmuir.5b00216>.
- [9] J. An, T. Usui, M. Logar, J. Park, D. Thian, S. Kim, et al., Plasma processing for crystallization and densification of atomic layer deposition BaTiO₃ thin films, *ACS Appl. Mater. Interfaces* 6 (2014) 10656–10660, <http://dx.doi.org/10.1021/am502298z>.
- [10] P. Schindler, Y. Kim, D. Thian, J. An, F.B. Prinz, Plasma-enhanced atomic layer deposition of BaTiO₃, *Scr. Mater.* (n.d.), doi:10.1016/j.scriptamat.2015.08.026.
- [11] H.B. Profijt, S.E. Potts, M.C.M. van de Sanden, W.M.M. Kessels, Plasma-assisted atomic layer deposition: basics, opportunities, and challenges, *J. Vac. Sci. Technol. A* 29 (2011) 050801, <http://dx.doi.org/10.1116/1.3609974>.
- [12] W. Heywang, Resistivity anomaly in doped barium titanate, *J. Am. Ceram. Soc.* 47 (1964) 484–490, <http://dx.doi.org/10.1111/j.1151-2916.1964.tb13795.x>.
- [13] Y.W. Yoo, W. Jeon, W. Lee, C.H. An, S.K. Kim, C.S. Hwang, Structure and electrical properties of Al-Doped HfO₂ and ZrO₂ films grown via atomic layer deposition on Mo electrodes, *ACS Appl. Mater. Interfaces* 6 (2014) 22474–22482, <http://dx.doi.org/10.1021/am506525s>.
- [14] H.J. Cho, Y.D. Kim, D.S. Park, E. Lee, C.H. Park, J.S. Jang, et al., New TIT capacitor with ZrO₂/Al₂O₃/ZrO₂ dielectrics for 60nm and below DRAMs, in: *Solid-state Device Res. Conf. 2006 ESSDERC 2006 Proceeding 36th Eur.*, 2006, pp. 146–149, <http://dx.doi.org/10.1109/ESSDERC.2006.307659>.
- [15] D.-S. Kil, H.-S. Song, K.-J. Lee, K. Hong, J.-H. Kim, K.-S. Park, et al., Development of new TiN/ZrO₂/Al₂O₃/ZrO₂/TiN capacitors extendable to 45nm generation DRAMs replacing HfO₂ based dielectrics, in: *2006 Symp. VLSI Technol. 2006 Dig. Tech. Pap.*, 2006, pp. 38–39, <http://dx.doi.org/10.1109/VLSIT.2006.1705205>.
- [16] Y.-H. Wu, C.-K. Kao, B.-Y. Chen, Y.-S. Lin, M.-Y. Li, H.-C. Wu, High density metal-insulator-metal capacitor based on ZrO₂/Al₂O₃/ZrO₂ laminate dielectric, *Appl. Phys. Lett.* 93 (2008) 033511, <http://dx.doi.org/10.1063/1.2958238>.
- [17] S.K. Kim, S.W. Lee, J.H. Han, B. Lee, S. Han, C.S. Hwang, Capacitors with an equivalent oxide thickness of <0.5 nm for nanoscale electronic semiconductor memory, *Adv. Funct. Mater.* 20 (2010) 2989–3003, <http://dx.doi.org/10.1002/adfm.201000599>.
- [18] T. Usui, S.A. Mollinger, A.T. Iancu, R.M. Reis, F.B. Prinz, High aspect ratio and high breakdown strength metal-oxide capacitors, *Appl. Phys. Lett.* 101 (2012) 033905, <http://dx.doi.org/10.1063/1.4737641>.
- [19] J.C. Wang, K.C. Chiang, T.F. Lei, C.L. Lee, Carrier transportation of rapid thermal annealed CeO₂ gate dielectrics, *Electrochem. Solid-State Lett.* 7 (2004) E55–E57, <http://dx.doi.org/10.1149/1.1819855>.
- [20] Y. Liu, H. Kim, J.-J. Wang, H. Li, R.G. Gordon, Effects of low temperature O₂ treatment on the electrical characteristics of amorphous LaAlO₃ films by atomic layer deposition, *ECS Trans.* 16 (2008) 471–478, <http://dx.doi.org/10.1149/1.2981628>.
- [21] S.A. Mojarad, K.S.K. Kwa, J.P. Goss, Z. Zhou, N.K. Ponn, D.J.R. Appleby, et al., A comprehensive study on the leakage current mechanisms of Pt/SrTiO₃/Pt capacitor, *J. Appl. Phys.* 111 (2012) 014503, <http://dx.doi.org/10.1063/1.3673574>.
- [22] F.D. Hideo Nakajima, Diffusion in α -Ti and Zr, *Mater. Trans.* 44 (2003) 2–13, <http://dx.doi.org/10.2320/matertrans.44.2>.

- [23] L. Fonseca, A. Knizhnik, First-principles calculation of the TiN effective work function on SiO₂ and on HfO₂, Phys. Rev. B 74 (2006), <http://dx.doi.org/10.1103/PhysRevB.74.195304>.
- [24] M. Kadoshima, T. Matsuki, S. Miyazaki, K. Shiraishi, T. Chikyo, K. Yamada, et al., Effective-work-function control by varying the TiN thickness in poly-Si/TiN gate electrodes for scaled high- CMOSFETs, IEEE Electron Device Lett. 30 (2009) 466–468, <http://dx.doi.org/10.1109/LED.2009.2016585>.
- [25] M. Vehkamäki, T. Hatanpää, M. Ritala, M. Leskelä, S. Väyrynen, E. Rauhala, Atomic layer deposition of BaTiO₃ thin films—effect of barium hydroxide formation, Chem. Vap. Depos. 13 (2007) 239–246, <http://dx.doi.org/10.1002/cvde.200606538>.
- [26] M.D. Groner, F.H. Fabreguette, J.W. Elam, S.M. George, Low-temperature Al₂O₃ atomic layer deposition, Chem. Mater. 16 (2004) 639–645, <http://dx.doi.org/10.1021/cm0304546>.
- [27] M.L. Huang, Y.C. Chang, C.H. Chang, T.D. Lin, J. Kwo, T.B. Wu, et al., Energy-band parameters of atomic-layer-deposition Al₂O₃/InGaAs heterostructure, Appl. Phys. Lett. 89 (2006) 012903, <http://dx.doi.org/10.1063/1.2218826>.
- [28] J.M. Lee, J.C. Shin, C.S. Hwang, H.J. Kim, C.-G. Suk, Preparation of high quality RuO₂ electrodes for high dielectric thin films by low pressure metal organic chemical vapor deposition, J. Vac. Sci. Technol. A 16 (1998) 2768–2771, <http://dx.doi.org/10.1116/1.581419>.